Optical and Quantum Electronics **25** *(1993) 1–25*

Spectral broadening of picosecond laser pulses in optical fibres

P. WEIDNER, A. PENZKOFER
Naturwissenschaftliche Fakultät II – Physik, Universität Regensburg, W-8400 Regensburg, Germany

Received 30 June; accepted 31 July 1992

Picosecond light pulses of a passively mode-locked ruby laser (pulse duration $\Delta t_L \approx 35$ ps) are spectrally broadened in optical fibres of core diameters from 4 μm to 600 μm. Combining the effects of self-phase modulation, stimulated Raman scattering, and parametric four-photon interaction in an 8-μm core fibre of 4 m length with the effect of selective spectral attenuation in a ruby rod resulted in rather smooth spectra extending from 685 nm to 830 nm (spectral width $\approx 2300\,\text{cm}^{-1}$).

1. Introduction

Time-resolved spectral studies in the vicinity of the pump laser frequency, like transient spectral hole burning [1, 2], require small-bandwidth ultrashort pump pulses and broadband probe pulses of equal centre frequency. The broadband probe pulses may be generated by passing part of the pump pulses through a Kerr medium causing self-phase modulation [3]. Optical fibres are most appropriate for spectral broadening by self-phase modulation because high intensities in a small spot are maintained over long distances [4–8]. In fibres the spectral broadening may be extended by cross-phase modulation [4, 5], modulation instability [4, 5, 9], stimulated Raman scattering [4, 5], stimulated four-photon mixing [4, 5, 10–13] and parametric amplification [4, 11, 14]. Strongly broadened spectral pulses in monomode fibres [7, 12, 13, 15, 16] and multimode fibres [17, 18] have been reported. The spectrally broadened pulses were often temporally shortened in pulse compression arrangements [19, 20].

In this paper we investigate the spectral broadening of picosecond ruby laser pulses in optical fibres of core diameters between 4 μm and 600 μm. The contributions of self-phase modulation, stimulated Raman scattering, and parametric four-photon interaction to the spectral shapes are analysed. Rather smooth spectra extending from 685 nm to 830 nm have been obtained by passing picosecond ruby laser pulses through an 8-μm core fibre of 4 m length and filtering the output in a 10-cm-long ruby rod.

2. Experimental

A schematic of the experimental setup is shown in Fig. 1. Picosecond pulse trains are generated in an active (acoustooptic modulator IntraAction model ML-50Q) and passive (saturable absorber 1,1′-diethyl-2,2′-dicarbocyanine iodide in methanol) mode-locked ruby laser. The wavelength is $\lambda_L = 694.3$ nm. Single pulses are separated by a

0306–8919

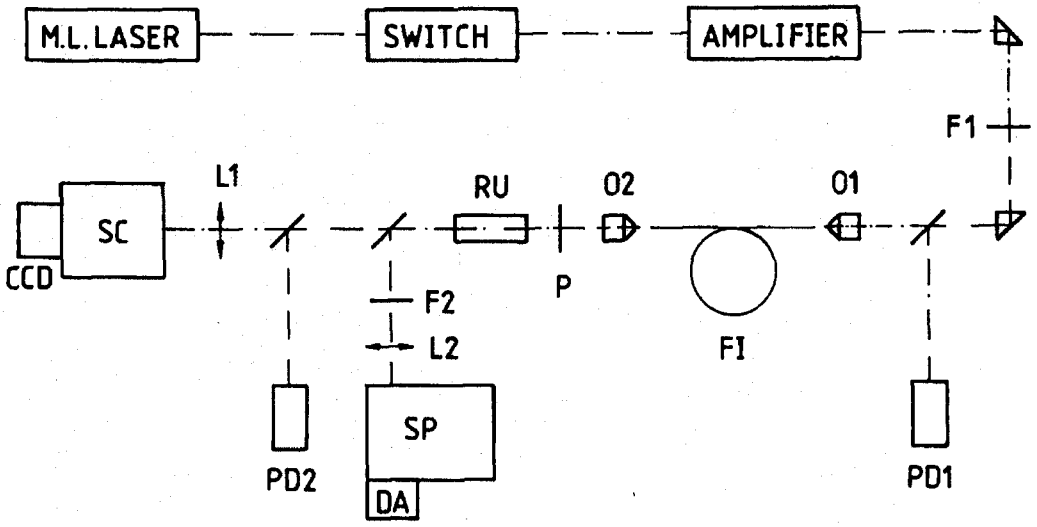

Figure 1 Experimental arrangement. F1, F2, neutral density filters; O1, O2, objectives; FI, fibre; P, polarizer; RU, ruby rod; L1, L2, lenses; SC, streak camera; CCD, CCD camera; PD1, PD2, photodetectors; SP, grating spectrometer; DA, diode array system.

Pockels cell shutter (Lasermetrics model 1071 FW Pockels cell and model 8601 C high-voltage pulse generator) and amplified by passing twice through a ruby amplifier. Behind the ruby amplifier the pulse duration is $\Delta t_L = 35 \pm 5\,\text{ps}$ (FWHM) and the spectral width is $\Delta\tilde{\nu}_L = 0.6 \pm 0.2\,\text{cm}^{-1}$ (FWHM). The pulse energy is varied by altering the power supply voltage of the amplifier and by inserting filters in the optical path.

The various fibres applied are listed in Table I. They are not polarization preserving. The input optics and the output optics were adjusted to the fibre core diameter. In some of the experiments a dichroitic polarizer and a ruby rod (0.05 wt% Cr^{3+}, c-axis at an angle of 60° to the rod axis, length 10 cm) were inserted behind the fibre in order to attenuate the spectrum at the central laser frequency. The polarizer was oriented parallel to the ordinary ray propagation through the rod where the central laser frequency is most strongly attenuated.

The input pulse energy was measured with photodetector PD1 and the light transmission through the fibres was determined with the photodetectors PD1 and PD2. The pulse spectra behind the fibres were registered with a 25-cm grating spectrometer (1800 grooves per mm and 600 grooves per mm) and a diode array system. The temporal shapes were measured with a streak camera (Hamamatsu type C1587 with fast streak plug-in type M1952).

3. Results

Typical pulse spectra obtained in various fibres are shown in Figs 2 to 7. The spectra are not corrected for the spectral sensitivity of the neutral density filters, the spectrometer and the silicon diode array detector.

The spectra of Fig. 2a and 2b belong to a 4-μm core fibre of 10 m length (no. 1 of Table I). In both cases the stimulated Raman scattering threshold is exceeded. The input pulse energies to the fibres W_i and output pulse energies from the fibres W_o are given in the figure caption. The spectrally broadened laser pulses of centre wavelength $\lambda_L = 694.3\,\text{nm}$ and the spectrally broadened first Stokes Raman pulses centred around $\lambda_R = 716\,\text{nm}$ (spectral Stokes shift $\delta\tilde{\nu}_R \approx 440\,\text{cm}^{-1}$ [6]) are seen. In Fig. 2c an output

TABLE I Fibre parameters of investigated single-step silica optical fibres. Wavelength $\lambda_L = 694.3\,nm$. Pulse duration $\Delta t_L = 35\,ps$

Fibre number	1	2	3	4	5	6
Type	F-SV[a]	F-SF[a]	F-SS[a]	HCP-M0125T-12[b]	HCL-M0200T-10[b]	HCP-M0600T-08[b]
Length l (m)	10	(a) 10, (b) 50	4	4	2	3.5
Core diameter d (μm)	4	5	8	125	200	600
Fundamental mode radius w_0 (μm)	2.8	2.8	3.5	40	63	189
Numerical aperture N_A	0.10	0.10	0.10	0.37	0.22	0.37
Single mode cut-off wavelength λ_c (μm)	0.523	0.653	1.045	60.4	57.5	290
Normalized frequency V	1.81	2.26	3.62	209	199	1005
Mode number M[c]	2	2	6	17700	16050	409350
Absorption coefficient α (cm^{-1})	$\sim 1.6 \times 10^{-5}$	$\sim 1.6 \times 10^{-5}$	$\sim 1.6 \times 10^{-5}$	$\sim 3 \times 10^{-5}$	$\sim 2 \times 10^{-5}$	$\sim 3 \times 10^{-5}$
Input optics power or focal length	20×	20×	20×	6 cm	15 cm	30 cm
Output optics power or focal length	4×	4×	4×	2.5 cm	2.5 cm	2.5 cm
Fibre transmission	0.05	0.05	0.11	0.15	0.27	0.44
Surface damage threshold energy $W_{sur,d}$ (J)[d]	3.7×10^{-6}	3.7×10^{-6}	5.8×10^{-6}	7.54×10^{-4}	1.87×10^{-3}	1.68×10^{-2}
Volume damage threshold energy $W_{bulk,d}$ (J)[e]	1.2×10^{-5}	1.2×10^{-5}	1.9×10^{-5}	2.4×10^{-3}	6×10^{-3}	5.4×10^{-2}

[a] From Newport Corporation.
[b] From Ensign-Bickford Optics Company.
[c] Orthogonal polarizations are counted.
[d] $\epsilon_{sur,d} = 15\,J\,cm^{-2}$ [25, 26], and $a_{eff} = w_0$ is assumed
[e] $\epsilon_{bulk,d} = 50\,J\,cm^{-2}$ [27] and $a_{eff} = w_0$ is assumed

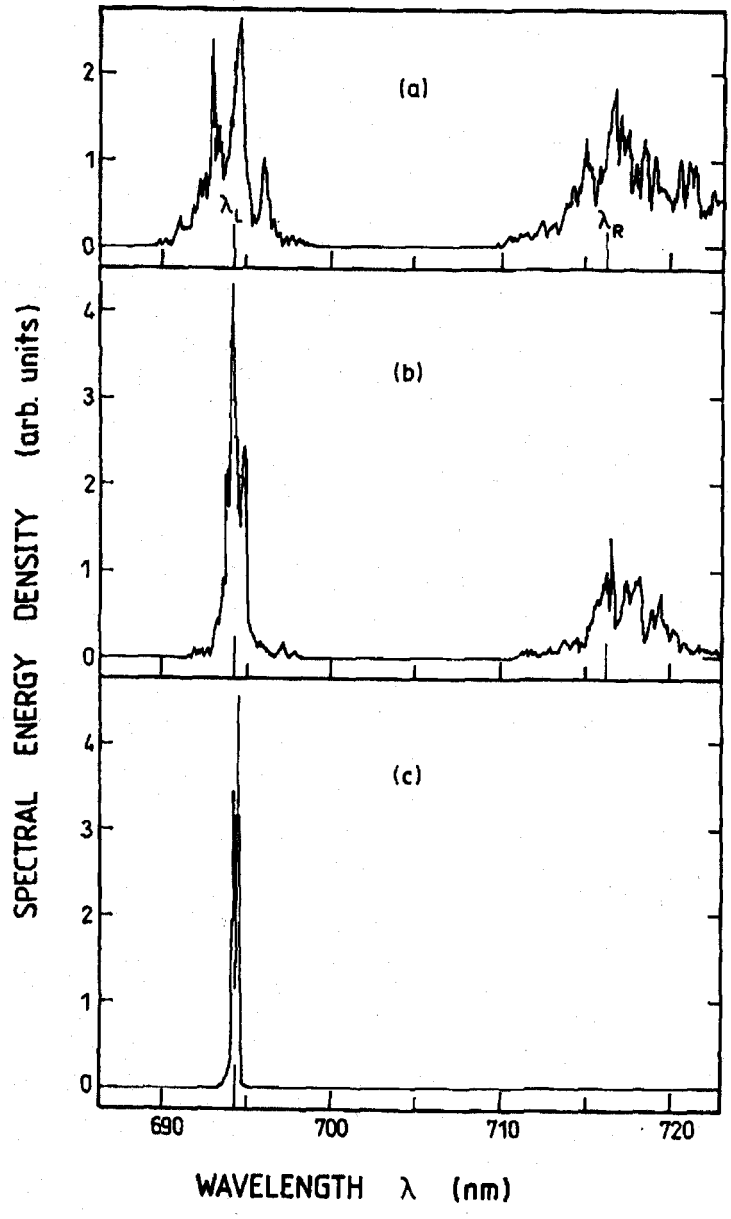

Figure 2 Examples of pulse spectra behind monomode fibres Spectra are taken without ruby filter. (a) Fibre no 1 (4-μm core diameter), input pulse energy $W_i = 1.1\,\mu$J, output pulse energy $W_o = 0.055\,\mu$J. (b) Fibre no 1, $W_i = 0.53\,\mu$J, $W_o = 0.027\,\mu$J (c) Fibre no. 2a (5-μm core diameter), $W_i = 0.14\,\mu$J, $W_o = 7$ nJ

spectrum of a 5-μm core fibre of 10 m length (no. 2a) is shown where the laser energy is below the stimulated Raman scattering threshold. The spectral distributions are similar for the 4-μm fibre and the 5-μm fibre in the case of equal laser energy density in the fibre core.

In Fig. 3 two spectra are shown for the 8-μm core fibre of 4 m length (no. 3). The ruby filter was inserted. Its transmission is indicated in Fig. 3a. The spectrum in Fig. 3a belongs to a pulse energy above the stimulated Raman scattering threshold. The spectral distribution spans the full wavelength region from λ_L to λ_R. At high enough pulse energies the spectrum extends out even to the wavelength of the fifth Stokes Raman component ($\lambda_{5R} = 819$ nm) at the long-wavelength side and to 685 nm at the

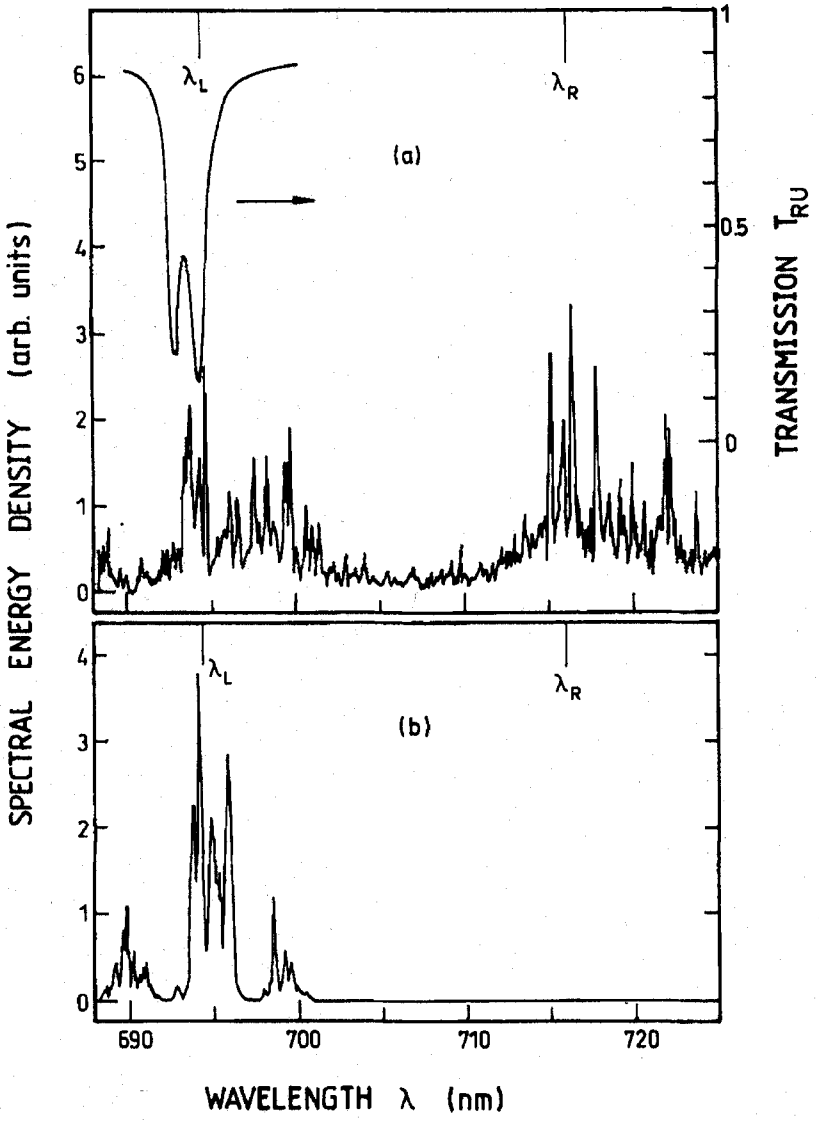

Figure 3 Examples of pulse spectra behind low-order-mode fibre no 3 (8-μm core diameter). Ruby filter is inserted. (a) $W_i = 3\,\mu J$, $W_o = 0.3\,\mu J$ (b) $W_i = 0.35\,\mu J$, $W_o = 0.035\,\mu J$. Transmission T_{RU} of ruby rod is indicated in (a).

short-wavelength side as shown in Fig. 6a. The combined effects of self-phase modulation, stimulated Raman scattering, and parametric four-photon interaction are responsible for the spectral extension (see discussion below). The spectrum in Fig. 3b is taken below the onset of stimulated Raman scattering. The side lobes at 690 nm and 698 nm are due to phase-matched parametric four-photon interaction (stimulated parametric four-wave mixing $\nu_L + \nu_L \rightarrow \nu_3 + \nu_4$ [4, 5, 10–13]; phase-matching is achieved by coupling of different modes in the low-order mode fibre [11, 21]).

The spectra shown in Fig. 4 and Fig. 6b belong to a 125-μm core fibre of 4 m length (no. 4). The spectrum in Fig. 4a (without ruby filter) is taken at an intensity before the onset of stimulated Raman scattering. The pulse is broadened by self-phase modulation. In Fig. 4b (with ruby filter) the self-phase-modulated laser pulse and the stimulated Raman pulse are seen. The lobes at the long-wavelength side of the ruby laser pulse

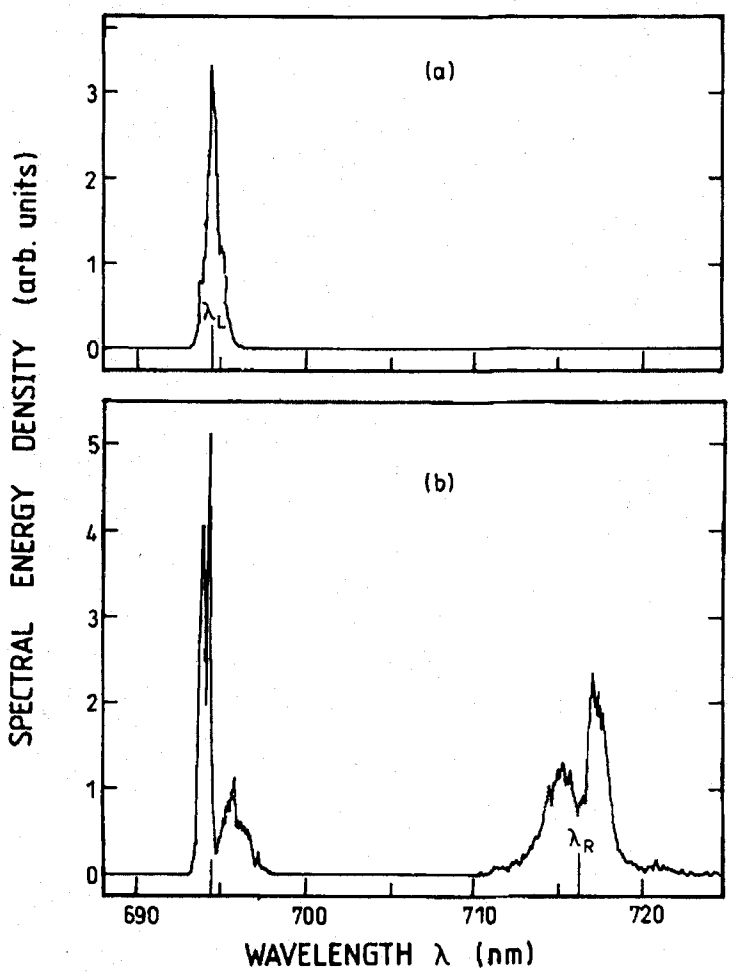

Figure 4 Examples of pulse spectra behind multimode fibre no. 4 (125-μm core diameter). (a) Without ruby filter. $W_i = 60\,\mu J$, $W_o = 8.5\,\mu J$. (b) Ruby filter is inserted. $W_i = 100\,\mu J$, $W_o = 15\,\mu J$.

and at the short-wavelength side of the stimulated Raman pulse are thought to be generated by the parametric four-photon interaction $\nu_L + \nu_R \rightarrow \nu_3 + \nu_4$ which is phase-matched by nonlinear refractive index contributions [4, 22, 23] (see discussion below; the process is also called modulation instability [9]). At somewhat higher input energies the first, second, third and even fourth Stokes Raman components are generated as shown in Fig. 6b.

The spectra in Fig. 5a and 5b belong to a 200-μm core fibre of 2 m length (no. 5). The spectrum (a) is taken before the onset of stimulated Raman scattering, while spectrum (b) is taken above the threshold of stimulated Raman scattering. The spectra of Fig. 5c and 6c belong to a 600-μm core fibre of 3.5 m length (no. 6). Raman light up to the fourth Stokes component is seen in Fig. 6c.

In Fig. 7 spectra are shown of a 5-μm core fibre of 50 m length (no. 2b). The spectral broadening of the laser pulse by self-phase modulation is enhanced before the onset of stimulated Raman scattering (Fig. 7a) because self-phase modulation acts over the full fibre length while the temporal overlap between laser light and first Stokes Raman light is limited to a walk-off distance of approximately 5.7 m (see discussion below). The spectrum of Fig. 7c shows efficient light generation at $\lambda_3 = 680$ nm and $\lambda_4 = 709$ nm

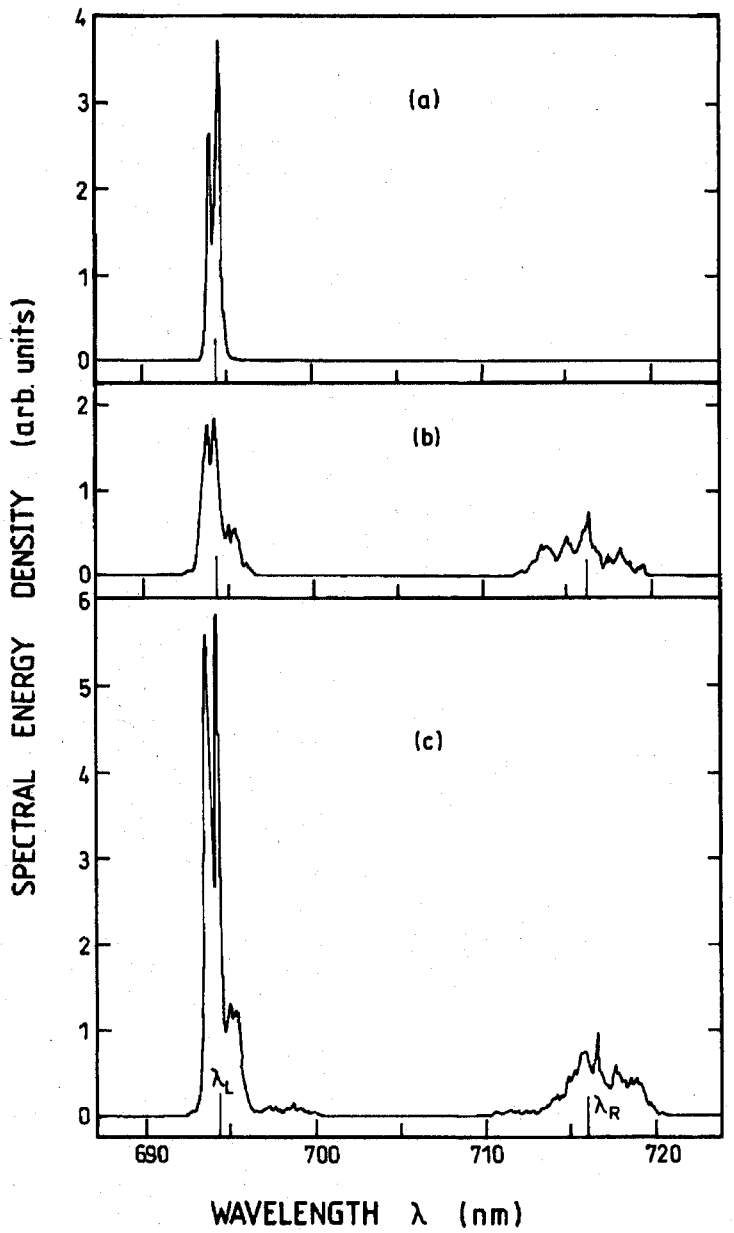

Figure 5 Examples of pulse spectra behind multimode fibres. Without ruby filter. (a) Fibre no. 5 (200-μm core diameter) with $W_i = 130\,\mu J$, $W_o = 35\,\mu J$. (b) Fibre no. 5 with $W_i = 220\,\mu J$, $W_o = 55\,\mu J$ (c) Fibre no. 6 (600-μm core diameter) with $W_i = 780\,\mu J$, $W_o = 310\,\mu J$.

due to phase-matched stimulated parametric four-photon interaction together with stimulated first Stokes Raman generation. The parametric idler light at 709 nm is larger than the signal light at 680 nm because of Raman amplification of the seeding idler light. It should be noted that Raman amplification occurs over a wide spectral range because the Raman gain curve of SiO_2 glass is very broad [6]. The fibre seems to support two fibre modes and the two-mode interaction allows phase matching. The theoretical cutoff wavelength of a 5-μm fibre is $\lambda_c = 653$ nm, but the real core diameter seems to be slightly larger. A core diameter of 5.32 μm is sufficient to support the fundamental mode HE_{11} and the second lowest modes TE_{01} and TM_{01} [24] (see discussion below). In

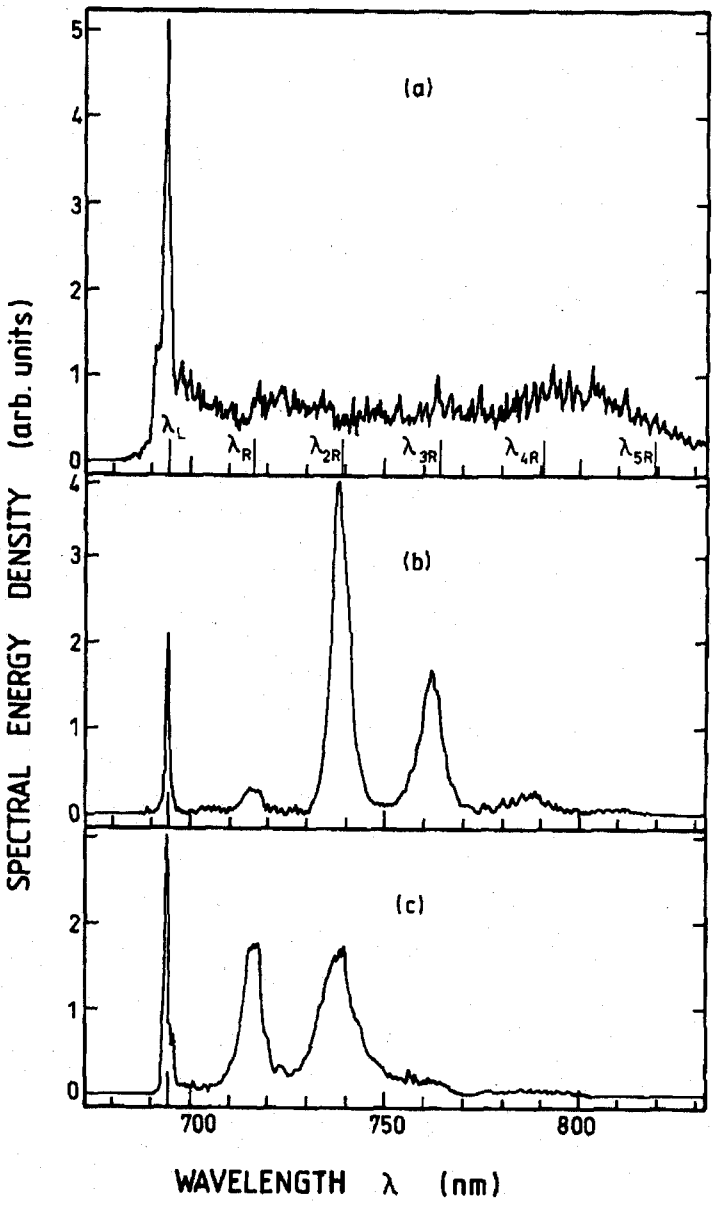

Figure 6 Examples of pulse spectra. Without ruby filter. (a) Fibre no. 3 (8 μm), $W_i = 5\,\mu J$, $W_o = 0.40\,\mu J$. (b) Fibre no. 4 (125 μm), $W_i = 400\,\mu J$, $W_o = 40\,\mu J$. (c) Fibre no. 6 (600 μm), $W_i = 800\,\mu J$, $W_o = 300\,\mu J$.

Fig. 7b a spectrum similar to that in Fig. 7c is shown which comprises the self-phase-modulated pump pulse, the stimulated four-wave mixing signal, and the first Stokes Raman signal.

In some of the spectra shown in the Figs 2 to 7 there is a small spike at exactly the ruby laser frequency. This spike is thought to be due to light passing through the fibre cladding and reaching the spectrometer. This false light might be avoided by using more tightly focusing input optics.

The experimental spectral halfwidths $\Delta\tilde{\nu}_L$ of the ruby laser pulses behind the various fibres are shown by symbols in Fig. 8 (ruby filter not inserted). The spectral broadening $\Delta\tilde{\nu}_L/\Delta\tilde{\nu}_{L,bwl}$ is indicated by the right ordinate ($\Delta\tilde{\nu}_{L,bwl}$ is the spectral width of a band-width-limited pulse). The data of Fig. 8 are displayed versus the total output pulse

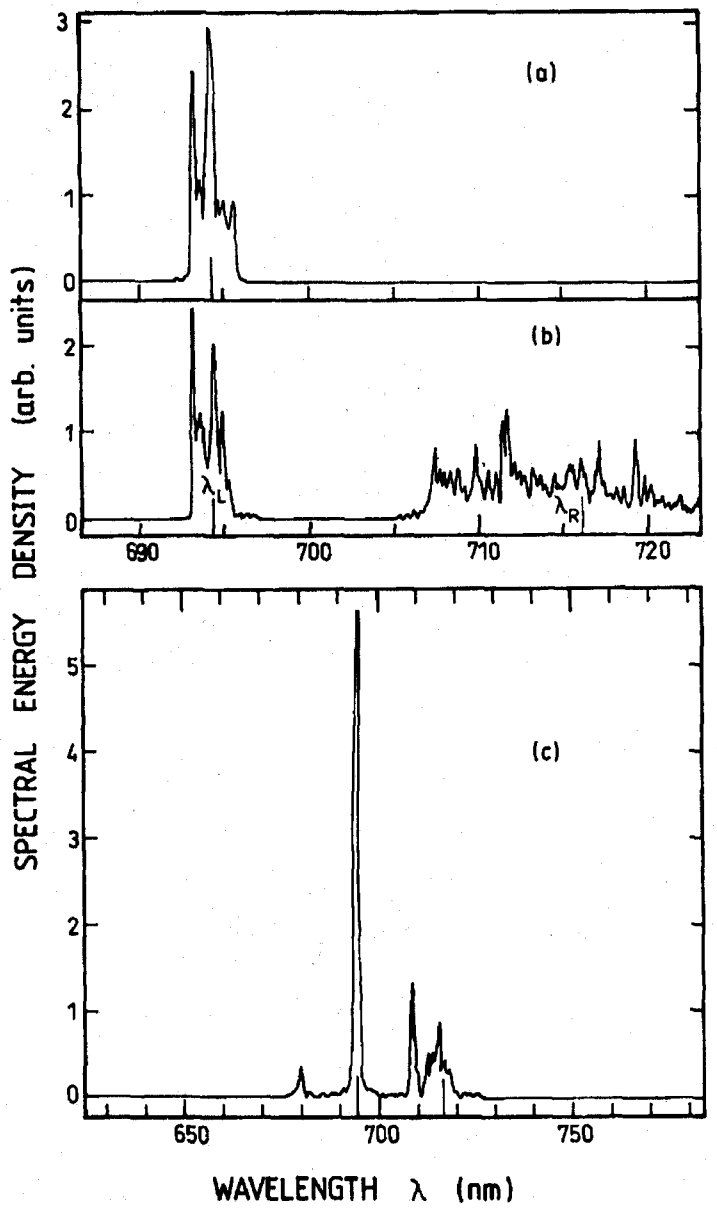

Figure 7 Pulse spectra obtained with fibre no. 2b (5-μm core diameter, 50 m length). Spectra are taken without ruby filter. (a) $W_i = 0.2\,\mu J$, $W_o = 0.01\,\mu J$. (b) $W_i = 0.26\,\mu J$, $W_o = 0.013\,\mu J$. (c) $W_i = 0.35\,\mu J$, $W_o = 0.017\,\mu J$

energy W_o behind the fibre, which is approximately equal to the laser pulse energy W_c in the core at the fibre entrance since losses in the fibre cores are negligible for the applied lengths. The experimental ratio of total output pulse energy to input pulse energy is listed in Table I. It indicates large input coupling losses for the used input optics. Increasing the numerical power (magnification) of the input objectives would allow increase in the energy throughput beyond 60%. The pulse energy needed for a certain spectral broadening scales approximately with the square of the core diameter. The fibre core diameter is selected according to the necessary energy of the spectrally broadened pulses. For example, a spectral broadening of $\Delta\nu_L/\Delta\nu_{L,bwl} = 20$ is achieved

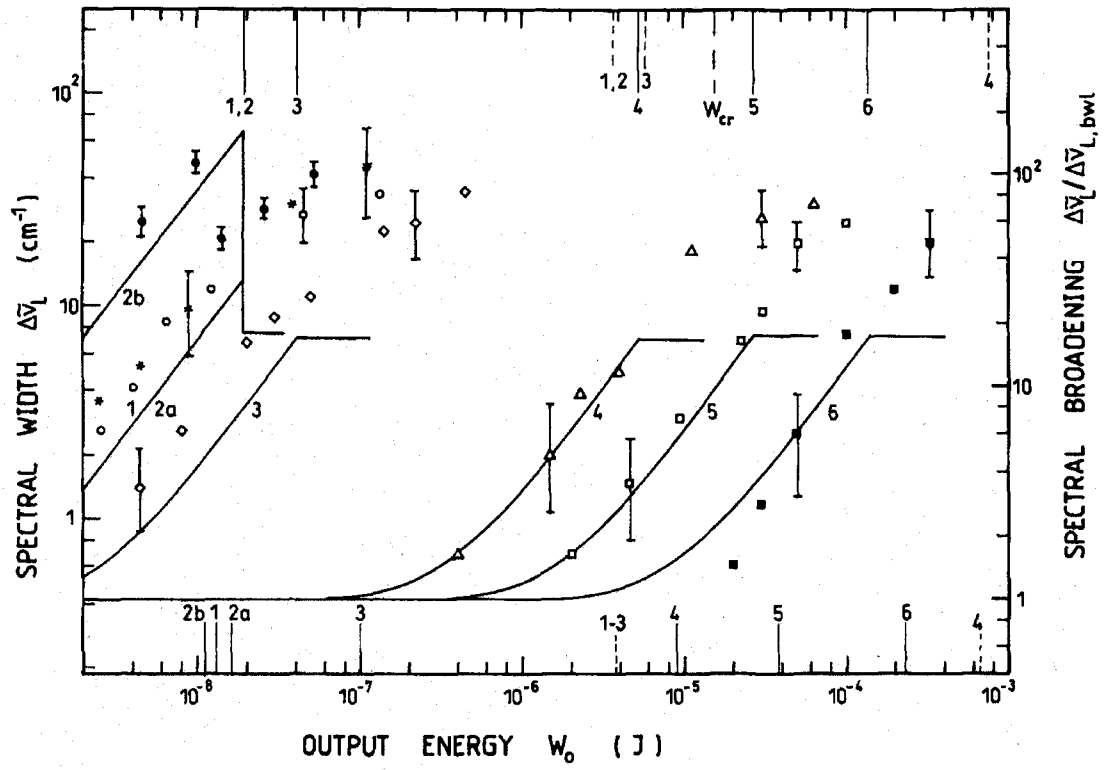

Figure 8 Dependence of spectral pulse width $\Delta\tilde{\nu}_L$ (FWHM) behind fibres on output pulse energy W_o (W_o assumed to be equal to pulse energy in fibre core). Ruby filter is not inserted. The numbers indicate the fibre numbers of Table I. The data points belong to (*) no. 1, (○) no 2a, (●) no. 2b, (◇) no 3, (△) no. 4, (□) no. 5, and (■) no. 6 The error bars indicate single-shot standard deviations. The curves are calculated spectral broadenings due to self-phase modulation (Equations 16 to 18 and 24). The solid bars along the upper abscissa indicate the theoretical Raman thresholds (Equation 21) and the solid bars along the lower abscissa show the experimental Raman thresholds. The dashed bars along the upper abscissa indicate theoretical surface damage thresholds. The dashed bars at the lower abscissa show experimental threshold surface damage energies. The dash-dotted bar at the upper abscissa indicates the theoretical critical self-focusing energy.

for $W_o \approx 10\,\text{nJ}$ in a 4-μm fibre of 10 m length and for $W_o \approx 150\,\mu\text{J}$ in a 600-μm fibre of 3.5 m length. Above the stimulated Raman scattering threshold the spectral broadening continues to increase with rising pulse energy (the exception is 50-m-long 5-μm core fibre). The experimental threshold energies of stimulated Raman scattering are indicated by the solid bars along the lower abscissa of Fig. 8. Spectral broadenings up to $\Delta\tilde{\nu}_L \approx 50\,\text{cm}^{-1}$ were obtained in the 5-μm core fibre of 50 m length before the onset of stimulated Raman scattering. Increasing the laser energy beyond the stimulated Raman scattering threshold in the 50-m-long fibre reduced the spectral broadening. The largest spectral broadening was achieved for the ruby-filtered
8-μm core fibre of 4 m length (not shown in Fig. 8). A long-wavelength shifted spectral width up to $2300\,\text{cm}^{-1}$ was obtained for $W_o \gtrsim 0.4\,\mu\text{J}$ (see smooth spectrum in Fig. 6a).

The maximum total output pulse energies $W_{o,max}$ are limited by material damage. On exceeding $W_{o,max}$, damage of the entrance surface was observed for the fibres of core diameter $d_c \leq 200\,\mu\text{m}$, while for the 600-$\mu$m fibre a bulk material damage occurred a few centimetres inside the fibre core. Experimental $W_{o,max}$ data are indicated by the dashed bars along the lower abscissa of Fig. 8. The surface damage energy density $\epsilon_{sur,d}$

of fused silica as a function of pulse duration is reported in [25, 26]. From these reports we deduce $\epsilon_{sur,d} \approx 15\,J\,cm^{-2}$ for our pulses of $\Delta t_L = 35\,ps$ duration. The expected surface damage energies, $W_{sur,d} \approx \pi a_{eff}^2 \epsilon_{sur,d}$, for the various fibres are listed in Table I and are indicated by the dashed bars along the upper abscissa of Fig. 8 (for the effective core radii a_{eff} see below). These $W_{sur,d}$ data agree reasonably well with the experimental $W_{o,max}$ data. The bulk damage energy density of pulses of 35 ps duration is approximately $\epsilon_{bulk,d} \approx 50\,J\,cm^{-2}$ (value deduced from data in [27]). The theoretical bulk threshold damage energies of the investigated fibres are listed in Table I. The bulk material damage observed at high input energies a few centimetres inside the 600-μm core fibre is caused by self-focusing (see discussion below).

The pulse duration behind the fibres was measured with a streak camera. When a ruby wavelength interference filter was put before the entrance to the streak camera, no temporal pulse broadening could be observed for the single-mode and low-order-mode fibres (nos 1 to 3) ($\Delta t_{L,o} = 35\,ps \pm 5\,ps$), while the multimode fibres broadened to a pulse duration of $\Delta t_{L,o} = 50 \pm 10\,ps$. Temporal spreading and multiple peaking was observed when the stimulated Raman light was not filtered off since the propagation speed of light increases with rising wavelength (normal dispersion of refractive index).

4. Discussion

Various nonlinear optical effects occur when intense picosecond light pulses pass through optical fibres [4, 5, 28, 29]. In the following, the relevant linear and nonlinear parameters are introduced and the nonlinear optical processes of self-phase modulation, stimulated Raman scattering, cross-phase modulation, parametric four-photon interaction, and self-focusing are described shortly and applied to interpret the experimental results.

4.1. Fibre characteristics

Some parameters and characteristic data of the applied fibres are collected in Tables I and II. The numerical aperture N_A is given by [30]

$$N_A = (n^2 - n_{cl}^2)^{1/2} = \sin \vartheta_0 \tag{1}$$

where n is the refractive index of the core, and n_{cl} is the refractive index of the cladding of the fibre. ϑ_0 is the maximum angle of incidence for which light is totally reflected in the fibre [16]. The normalized frequency V (characteristic waveguide parameter [24]) is defined by [30]

$$V = kaN_A = (2\pi/\lambda)\, aN_A \tag{2}$$

where $k = 2\pi/\lambda$ is the wave propagation constant, λ is the wavelength in vacuum, and a is the core radius. For $V \leq V_c = 2.405$ a step-index fibre supports only a single mode (fundamental mode HE_{11} with two orthogonal polarization directions). Therefore the cutoff wavelength λ_c for single-mode propagation is

$$\lambda_c = (2\pi/V_c)\, aN_A \tag{3}$$

For $\lambda < \lambda_c$ the approximate total number of modes M (including the mutually orthogonal polarizations) that can exist in a step-index fibre is [30]

$$M = 4V^2/\pi^2 \tag{4}$$

TABLE II Linear and nonlinear characteristic parameters of investigated non-polarization-maintaining silica optical fibres. Wavelength $\lambda_L = 694.3\,\text{nm}$. Duration $\Delta t_L = 35\,\text{ps}$. The relations $\gamma_2'/\gamma_2 = n_2'/n_2 = \gamma_I'/\gamma_I = g_P'/g_P = 5/6$, and $g_R'/g_R = 0.5$ are used [7, 33, 38]

Parameter	Value	References
Field coefficient of nonlinear refractive index n_2'	$1.03 \times 10^{-22}\,\text{m}^2\,\text{V}^{-2}$	[7, 38]
Intensity coefficient of nonlinear refractive index γ_2'	$2.67 \times 10^{-20}\,\text{m}^2\,\text{W}^{-1}$	Equation 11
Effective Raman gain coefficient g_R'	$1.4 \times 10^{-13}\,\text{mW}^{-1}$	[6] corrected for λ_L, ($g_R(\lambda) \propto \lambda^{-1}$ [39])
Long-fibre Raman threshold intensity $I_{R,th}$	$2.0 \times 10^9\,\text{W cm}^{-2}$	Equation 20, $L_R = L_{w,R}$
Peak parametric gain factor g_P'	$2.42 \times 10^{-13}\,\text{mW}^{-1}$	Equation 53
Pump loss distance L_α	$\approx 500\,\text{m}$	$L_\alpha = \alpha_L^{-1}$
Inverse of group velocity dispersion k_L''	$4.567 \times 10^{-26}\,\text{m}^{-1}\,\text{s}^2$	$k_L'' = \partial^2 k/\partial\omega^2\|_{\omega=\omega_L}$
Inverse of group velocity dispersion $D(\lambda)$	$1.784 \times 10^{-4}\,\text{s m}^{-2}$ $= 178.4\,\text{ps km}^{-1}\,\text{nm}^{-1}$	$D(\lambda) = \partial v_g^{-1}/\partial\lambda_L$
Dispersion length L_d	9.744 km	Equation 8
Soliton period z_0	15.306 km	Equation 9
Raman walk-off length $L_{w,R}$	5.7 m	Equation 7
Nonlinearity coefficient γ_I'	$2.42 \times 10^{-13}\,\text{mW}^{-1}$	Equation 12
Critical self-focusing power P_{cr}	$4.1 \times 10^5\,\text{W}$	Equation 56
Critical self-focusing energy W_{cr}	$15.4\,\mu\text{J}$	Equation 57

The effective beam radius w_0 of the fundamental mode in the fibre depends on V and is given by [31]

$$w_0 = \beta(V)a \tag{5}$$

where $\beta(V)$ is a decreasing function of V ($\beta(2.6) \approx 1$, $\beta(\infty) \approx 0.63$).

The absorption coefficients α_L of the applied fibres at the ruby laser wavelength are given in Table I. They are derived from attenuation data given by the fibre suppliers. The pump loss distance $L_\alpha = \alpha_L^{-1}$ is typically of the order of 500 m. It is much longer than the applied fibre lengths and therefore plays no role in our investigations.

The refractive indices of the fibre cores are assumed to be equal to the refractive indices of fused silica. The refractive indices $n(\lambda)$ are calculated by use of the dispersion formula given in [32]. They are displayed in Fig. 9b.

The group refractive index n_g is given by [4]

$$n_g = n + \omega(\partial n/\partial\omega) \tag{6}$$

where $\omega = 2\pi\nu = 2\pi c_0/\lambda$ is the angular frequency and c_0 is the vacuum light velocity. $n_g(\lambda)$ is plotted in Fig. 9a.

Two pulses of duration Δt_L and of wavelengths λ_L and λ overlap temporally only within the walk-off distance L_w given by [4]

$$L_w = \frac{t_0}{|v_g^{-1}(\lambda_L) - v_g^{-1}(\lambda)|} \tag{7}$$

where $t_0 = \Delta t_L/[2(\ln 2)^{1/2}]$ is half the 1/e pulse width and $v_g = c_0/n_g$ is the group velocity. $L_w(\lambda)$ is displayed in Fig. 9c for $\lambda_L = 694.3\,\text{nm}$ and $\Delta t_L = 35\,\text{ps}$. At the first Raman Stokes wavelength $\lambda_R = 716\,\text{nm}$ the walk-off length is $L_{w,R} = L_w(\lambda_R) = 5.7\,\text{m}$.

The effective interaction length of stimulated Raman scattering L_R is therefore limited to $L_R = \min(l, L_{w,R})$, where l is the fibre length [33, 34]. When self-phase modulation generates a spectral width of $\Delta\tilde{\nu}_L$ then $L_w(\tilde{\nu}_L + \Delta\tilde{\nu}_L/2)$ determines a critical length of optical wave-breaking (group velocity dispersion modifies temporal shape of self-phase-modulated pulse) [35]. The curve in Fig. 9c gives critical lengths of 90 m for $\Delta\tilde{\nu}_L = 50\,\text{cm}^{-1}$, and 50 m for $\Delta\tilde{\nu}_L = 100\,\text{cm}^{-1}$.

The temporal pulse broadening of initially bandwidth-limited non-self-phase-modulated pulses by group velocity dispersion is characterized by the dispersion length L_d

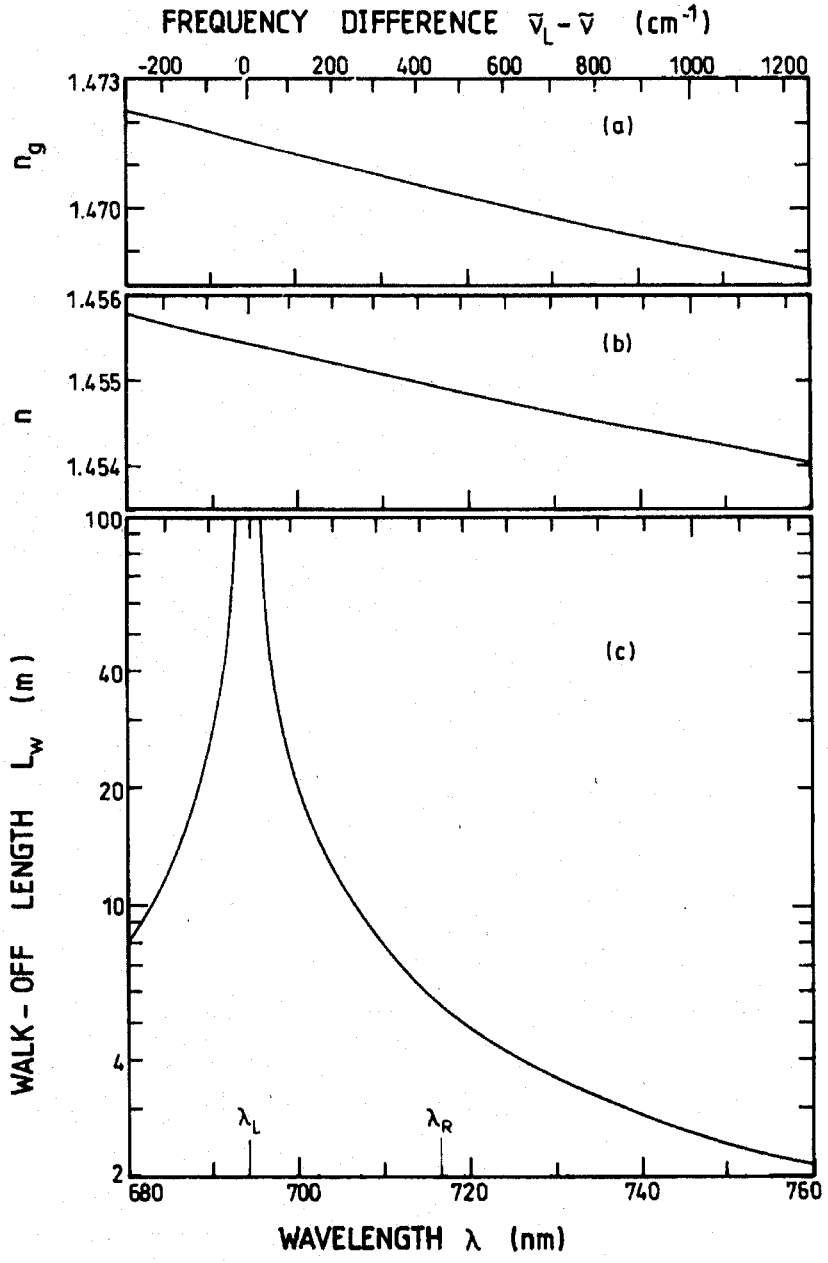

Figure 9 Wavelength dependences of (a) the group refractive index n_g (Equation 6), (b) the phase refractive index n [32], and (c) the walk-off length L_w (Equation 7, $\Delta t_L = 35$ ps)

which is given by [4, 33]

$$L_d = t_0^2/k_L'' = -(2\pi c_0/\lambda_L^2)\,(t_0^2/D(\lambda_L)) \tag{8}$$

where $k_L'' = \partial^2 k/\partial\omega^2 = \partial v_g^{-1}/\partial\omega$ at $\omega = \omega_L$ is the inverse of the group velocity dispersion in frequency space, and $D(\lambda_L) = \partial v_g^{-1}/\partial\lambda_L = -(2\pi c_0/\lambda_L^2)k_L''$ is the inverse group velocity dispersion in wavelength space. $\omega_L = 2\pi\nu_L = 2\pi c_0/\lambda_L$ is the angular frequency of the laser. An initially bandwidth-limited Gaussian pulse propagating a distance of L_d is temporally broadened by a factor of $2^{1/2}$ [4]. In our case the dispersion length is much longer than the applied fibre lengths ($L_d \approx 10\,\text{km}$, see Table II). The soliton period is [4]

$$z_0 = (\pi/2)L_d \tag{9}$$

The fibre nonlinearity may be expressed by the intensity-dependent change of the refractive index. This refractive index change is [3]

$$\Delta n = (n_2/2)|E_L|^2 = \gamma_2 I_L \tag{10}$$

where n_2 is the electric field coefficient of the nonlinear refractive index, $\gamma_2 = n_2/(n_L\epsilon_0 c_0)$ is the intensity coefficient of the nonlinear refractive index, n_L is the linear refractive index, E_L is the electric field amplitude, and I_L is the light intensity. ϵ_0 is the permittivity of vacuum. The relation between the nonlinear refractive index coefficient n_2 and the third-order nonlinear susceptibility $\chi^{(3)}_{xxxx}(-\omega_L;\omega_L,-\omega_L,\omega_L)$ is [36]

$$n_2 = n_L\epsilon_0 c_0\gamma_2 = (3/n_L)\chi^{(3)}_{xxxx}(-\omega_L;\omega_L,-\omega_L,\omega_L) \tag{11}$$

n_2 and γ_2 are listed in Table II. The nonlinearity coefficient γ_I is [4]

$$\gamma_I = k_L\gamma_2 = \omega_L\gamma_2/c_0 \tag{12}$$

In non-polarization-maintaining fibres the effective nonlinear refractive index coefficients are $n_2' = (5/6)n_2$, $\gamma_2' = (5/6)\gamma_2$, and the nonlinearity coefficient is reduced to $\gamma_I' = (5/6)\gamma_I$ [38].

The nonlinearity length L_{nl} is defined by $k_L\,\Delta n L_{nl} = \gamma_I I_L L_{nl} = 1$ [4], giving

$$L_{nl} = 1/\gamma_I I_L \tag{13}$$

For fibre lengths $l > L_{nl}$, nonlinear optical effects like self-phase modulation become important. In Fig. 10 the nonlinearity length L_{nl} is displayed versus the laser intensity I_L for non-polarization-maintaining fibres.

The soliton order N is given by [4]

$$N = (L_d/L_{nl})^{1/2} \tag{14}$$

The critical distance of nonlinear optical pulse deformation L_{def} is [4, 35]

$$L_{def} = (z_0/N) = (\pi/2)(L_d L_{nl})^{1/2} = (\pi/2)\left(\frac{L_d}{\gamma_I I_L}\right)^{1/2} \tag{15}$$

For $l > L_{def}$ optical wave-breaking occurs by the interplay of positive self-phase modulation and positive group velocity dispersion [33, 35]. The dependence of L_{def} on the laser intensity for non-polarization-maintaining fibres is displayed in Fig. 10.

4.2. Self-phase modulation

The spectral width of self-phase-modulated pulses (FWHM) is given approximately by [3, 39]

$$\Delta\nu_L = (\Delta\nu_{L,bwl}^2 + \Delta\nu_{SPM}^2)^{1/2} \tag{16}$$

with

$$\Delta\nu_{L,bwl} = 0.441/\Delta t_L \tag{17}$$

and

$$\Delta\nu_{SPM} = \frac{\nu_{0L} L_{SPM}}{c_0}\left(\frac{\partial\Delta n}{\partial t}\bigg|_{max} - \frac{\partial\Delta n}{\partial t}\bigg|_{min}\right) = \frac{\nu_{0L} L_{SPM}\gamma_2}{c_0}\left(\frac{\partial I_L}{\partial t}\bigg|_{t=-t_{0L}} - \frac{\partial I_L}{\partial t}\bigg|_{t=t_{0L}}\right)$$
$$= \frac{4(2\ln 2)^{1/2}\exp(-1/2)\nu_{0L}\gamma_2 I_{0L} L_{SPM}}{c_0\,\Delta t_L} \tag{18}$$

where $\Delta\nu_{L,bwl}$ is the spectral width of a bandwidth-limited Gaussian pulse of duration Δt_L (FWHM), and $\Delta\nu_{SPM}$ is the spectral broadening due to self-phase modulation. ν_{0L} is the central laser frequency and I_{0L} is the peak intensity of the laser pulse. L_{SPM} is the

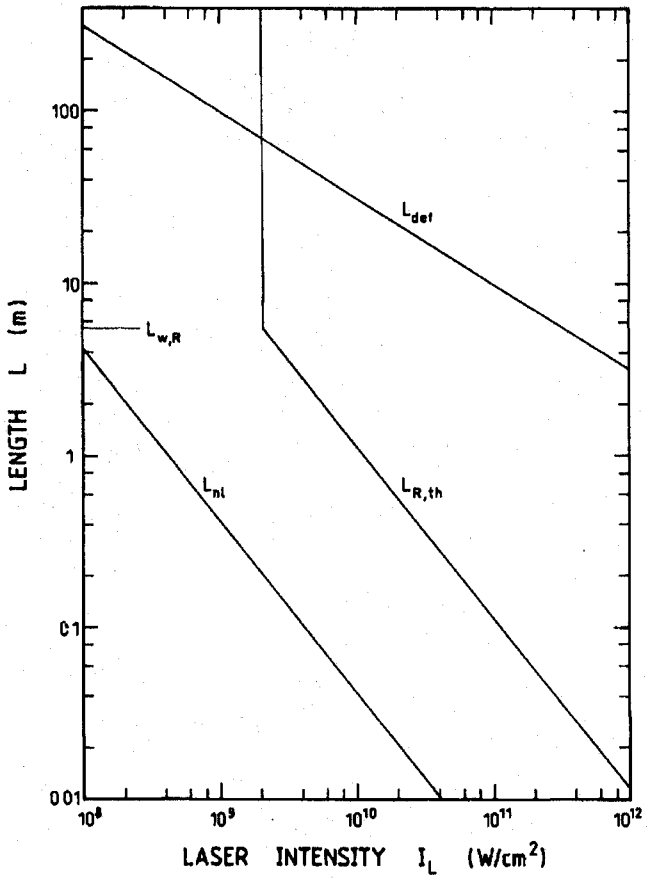

Figure 10 Dependence of the nonlinearity length L_{nl} (Equation 13), the Raman threshold length $L_{R,th}$ (Equation 22), and the optical wave-breaking length L_{def} (Equation 15) on the laser intensity in the fibre core

interaction length for self-phase modulation in the fibre. It is $L_{SPM} = \min(l, L_{R,th})$ where $L_{R,th}$ is the threshold length for efficient stimulated Raman scattering (see next section). The peak laser intensity I_{0L} is related to the laser pulse energy in the fibre core W_c by

$$I_{0L} = 2(\ln 2)^{1/2} W_c/(\pi^{3/2} \Delta t_L a_{eff}^2) \tag{19}$$

where a_{eff} is the effective core radius. In single-mode fibres it is $a_{eff} = w_0$ (Equation 5). In our calculations we use $a_{eff} = w_0$ even for multimode fibres. The pulse energy in the fibre core, W_c, is approximately equal to the output pulse energy of the fibre, W_o.

The solid curves in Fig. 8 represent theoretical spectral widths $\Delta\tilde{\nu}_L$ (left ordinate, Equation 16) and spectral broadenings $\Delta\tilde{\nu}_L/\Delta\tilde{\nu}_{L,bwl}$ (right ordinate) for the various investigated fibres. Before the onset of stimulated Raman scattering the experimental spectral widths agree reasonably well with the experimental data points. For the monomode fibre and the low-order-mode fibre the spectral broadening is slightly larger than expected, while for the multimode fibre it is nearly equal to expectations. For the multimode fibres the beam profile may be spatially more rectangular-shaped, leading to lower peak intensities and smaller spectral broadening. The spatial beam profile at the multimode fibre output was monitored by magnified imaging (linear amplification of 4) to a diode array system. A nearly rectangular profile was observed.

Before the onset of stimulated Raman scattering the self-phase-modulated pulses of spectral width $\Delta\nu_L$ should be compressible down to durations of $\Delta t_{L,com} \approx 0.5/\Delta\nu_L$ in pulse compression arrangements [19, 20, 33, 34].

4.3. Stimulated Raman scattering

In non-polarization-maintaining fibres efficient first Stokes stimulated Raman scattering occurs when the laser intensity exceeds a threshold intensity $I_{R,th}$ given by [6]

$$I_{R,th} = 16/g'_R L_R = 32/g_R L_R \tag{20}$$

where g_R is the Raman gain coefficient (see Table II) and $L_R = \min(l, L_{w,R})$ is the effective interaction length of stimulated Raman scattering (see above). $g'_R = g_R/2$ is the effective Raman coefficient of non-polarization-preserving fibres. The corresponding threshold laser energy $W_{R,th}$ is

$$W_{R,th} = \frac{8\pi^{3/2}}{(\ln 2)^{1/2}} \frac{\Delta t_L a_{eff}^2}{g'_R L_R} \tag{21}$$

The theoretical $W_{R,th}$ values according to Equation 21 are shown in Fig. 8 for the various applied fibres by the solid bars at the upper abscissa, while the experimental threshold energies of efficient stimulated Raman scattering are indicated by the solid bars along the lower abscissa. The experimental and theoretical thresholds agree reasonably well for the monomode fibres. For the 8-μm core fibre the experimental stimulated Raman scattering threshold energy is a factor of approximately 2.5 higher than the theoretical value. In this low-order-mode fibre stimulated four-wave mixing sets in before stimulated Raman scattering and reduces the pump laser intensity. For the multimode fibres (nos 4 to 6) the experimental Raman threshold energies are a factor of approximately 1.5 higher than the theoretical Raman threshold energies, indicating that the experimental effective beam radius a_{eff} is slightly larger than W_o used in the theor-

etical calculations (spatial beam profile is more rectangular-shaped). Also, temporal pulse broadening in the multimode fibres increases the Raman threshold energy.

If the laser intensity is increased beyond the Raman threshold intensity ($I_{0L} > I_{R,th}$, laser energy $W_o > W_{R,th}$) then a depletion of laser light sets in at a penetration distance of

$$L_{R,th} = \frac{16}{g'_R I_{0L}} = \frac{8\pi^{3/2}\Delta t_L a_{eff}^2}{(\ln 2)^{1/2} g'_R W_o} \tag{22}$$

according to Equations 20 and 21. The interaction length of efficient self-phase modulation is limited to the threshold length of efficient stimulated Raman scattering $L_{R,th}$ because for $l > L_{R,th}$ the peak pulse intensity I_{0L} is reduced. The Raman threshold length $L_{R,th}$ versus laser intensity is displayed in Fig. 10. Above the Raman threshold the nonlinear length L_{nl} is related to $L_{R,th}$ by

$$L_{nl} = 1/\gamma'_I I_{0L} = (g'_R/16\gamma'_I) L_{R,th} \tag{23}$$

Using the parameters of Table II gives $L_{nl} \approx 0.036 L_{R,th}$ (see Fig. 10).

When stimulated Raman scattering occurs, the spectral broadening by self-phase modulation is limited to

$$\Delta\nu_{SPM,R} = 64(2 \ln 2)^{1/2} \exp(-1/2)\nu_{0L}\gamma'^2_2/(c_0 \Delta t_L g'_R) \tag{24}$$

as is seen by insertion of Equation 22 in Equation 18. For fibre length $l > L_R$ the spectral broadening by self-phase modulation, $\Delta\nu_{SPM}$, drops down to $\Delta\nu_{SPM,R}$. In Fig. 8 the continuing experimental spectral broadening above the Raman threshold is thought to be due to cross-phase modulation and parametric four-photon interaction as is discussed in the following sections.

A spectral broadening $\Delta\nu_{SPM} > \Delta\nu_{SPM,R}$ by self-phase modulation is only possible if stimulated Raman scattering is avoided, as in the experiments with fibre no. 2b (curve 2b and dots • in Fig. 8) where $l \gg L_{w,R}$, and I_{0L} is slightly below $I_{R,th} = 16/(g'_R L_{w,R})$. The fibre length should be kept below L_{def} to avoid optical wave-breaking of the self-phase-modulated pulses.

4.4. Cross-phase modulation induced by stimulated Raman scattering

The effects of cross-phase modulation in fibres are discussed in detail in chapter 7 of [4] and in [5]. The presence of a stimulated Raman pulse influences the field-induced refractive index change Δn at the laser frequency ν_L according to

$$\Delta n(t) = \gamma_{2,LL} I_L(t) + \gamma_{2,LR} I_R(t) = (1/n_L \epsilon_0 c_0)\left[n_{2,LL} I_L(t) + n_{2,LR} I_R(t)\right] \tag{25}$$

with $\gamma_{2,LR} = 2\gamma_{2,LL} = 2\gamma_2$ and $n_{2,LR} = 2n_{2,LL} = 2n_2$ [4, 5]. The spectral broadening becomes

$$\Delta\nu_{PM} = \Delta\nu_{SPM} + \Delta\nu_{XPM} \tag{26}$$

with

$$\Delta\nu_{XPM} \approx \frac{2\nu_{0L}\gamma_2}{c_0}\left(\int_{L_{R,th}}^{l} \frac{\partial I_R}{\partial t}\bigg|_{t=-t_{0L}} dz - \int_{L_{R,th}}^{l} \frac{\partial I_R}{\partial t}\bigg|_{t=t_{0L}} dz\right) \tag{27}$$

and $\Delta\nu_{SPM}$ given by Equation 18.

The contribution $\Delta\nu_{XPM}$ is reduced because the length of efficient Raman signal presence $l - L_{R,th}$, is shorter than the fibre length l, and because the temporal walk-off between the Raman pulse and the laser pulse reduced $\partial I_R/\partial t|_{t=-t_{0L}}$ and $\partial I_R/\partial t|_{t=t_{0L}}$. The temporal shift between pump pulse and Raman pulse causes an asymmetric spectral broadening by cross-phase modulation.

4.5. Optical wave-breaking

Optical wave-breaking of the self-phase-modulated pulses is not expected for the short fibres of length $l < L_{w,R}$. In this case it is $L_{def}/L_{R,th} \gg 1$ as is seen in Fig. 10. Since high laser intensity is restricted to a length of the order of $L_{R,th}$, no optical wave-breaking is expected. For fibre no. 2b of 50 m length at $I_{L,max} = 16/(g'_R L_{w,R})$ we estimate a minimum deformation length of $L_{def,min} = (\pi/2)(L_d/\gamma'_1 I_{L,max})^{1/2} = 70\,\text{m}$. Here $L_{def,min}$ is still longer than the fibre length l. The measured spectra (Fig. 7) give no indication of optical wave-breaking [35] (no spectral wings on self-phase-modulated pulses are seen).

4.6. Parametric four-photon interaction

In fibres the partially degenerate parametric four-photon interaction (I) $\omega_L + \omega_L \rightarrow \omega_3 + \omega_4$ may occur. If two pulses at ω_L and ω_R are present the nondegenerate four-photon interaction (II) $\omega_L + \omega_R \rightarrow \omega_3 + \omega_4$ is possible as well. If no signal at ω_3 and ω_4 is entered to the fibre, one speaks of stimulated four-photon mixing [4, 5, 13, 40–43], stimulated parametric four-photon interaction [44, 45], stimulated four-wave parametric emission [46], or parametric four-photon generation (start from quantum noise and black-body radiation [37]). If a weak signal at either ω_3 or ω_4 is already present, one speaks of four-photon parametric amplification [4, 5, 10, 47].

In the absence of absorption and if the field strengths E_3 and E_4 are much less than E_L and E_R, the equation system for the four-photon interaction $\omega_L + \omega_R \rightarrow \omega_3 + \omega_4$ reads [10]:

$$\partial E_3/\partial z = -(i3\omega_3/2n_3c_0)\Big[D\chi^{(3)}_{xxxx}(-\omega_3;\omega_L,\omega_R,-\omega_4)E_L E_R E_4^* \exp(i\Delta kz) + 2\chi^{(3)}_{xxxx}(-\omega_3;\omega_L,-\omega_L,\omega_3)|E_L|^2 E_3 + 2\theta\chi^{(3)}_{xxxx}(-\omega_3;\omega_R,-\omega_R,\omega_3)|E_R|^2 E_3\Big] \tag{28}$$

$$\partial E_4/\partial z = -(i3\omega_4/2n_4c_0)\Big[D\chi^{(3)}_{xxxx}(-\omega_4;\omega_L,\omega_R,-\omega_3)E_L E_R E_3^* \exp(i\Delta kz) + 2\chi^{(3)}_{xxxx}(-\omega_4;\omega_L,-\omega_L,\omega_4)|E_L|^2 E_4 + 2\theta\chi^{(3)}_{xxxx}(-\omega_4;\omega_R,-\omega_R,\omega_4)|E_R|^2 E_4\Big] \tag{29}$$

$$E_L(z) = E_L(0)\exp(-i\delta k_L z) \tag{30}$$

$$E_R(z) = E_R(0)\exp(-i\delta k_R z) \tag{31}$$

with

$$\delta k_L = (\omega_L/c_0)\gamma_2 (I_L + 2\theta I_R) \tag{32}$$

$$\delta k_R = (\omega_R/c_0)\gamma_2 (DI_L + \theta I_R) \tag{33}$$

and

$$\Delta k = k_3 + k_4 - k_L - k_R \tag{34}$$

$D = 2$ and $\theta = 1$ for $\omega_R \neq \omega_L$; and $D = 1$, $\theta = 0$ and $I_R = I_L$ for $\omega_R = \omega_L$. For non-polarization-maintaining fibres γ_2 and $\chi^{(3)}$ have to be replaced by $\gamma_2' = (5/6)\gamma_2$ and $\chi^{(3)\prime} = (5/6)\chi^{(3)}$ [7, 38].

For a crude analysis all third-order nonlinear susceptibilities $\chi^{(3)}$ are assumed to be real and equal, all refractive indices are set to n_L, all frequencies are approximated by ω_L, and E_L and E_R are assumed to be real. Using the relations $n_2 = 3\chi^{(3)}/n_L$, $\gamma_2 = n_2/(n_L\epsilon_0 c_0)$, $I_L = (n_L\epsilon_0 c_0)|E_L|^2/2$, and $\gamma_I = \gamma_2\omega_L/c_0$, Equations 28 and 29 reduce to

$$\partial E_3/\partial z = -i\gamma_I\left[D(I_L I_R)^{1/2}E_4^* \exp[i(\Delta k = \delta k_L - \delta k_R)z] + 2(I_L + \theta I_R)E_3\right] \tag{35}$$

$$\partial E_4/\partial z = -i\gamma_I\left[D(I_L I_R)^{1/2}E_3^* \exp[i(\Delta k - \delta k_L - \delta k_R)z] + 2(I_L + \theta I_R)E_4\right] \tag{36}$$

Using the relations

$$A_3 = E_3 \exp(-i\delta k_3 z) \tag{37}$$

$$A_4 = E_4 \exp(-i\delta k_4 z) \tag{38}$$

with

$$\delta k_3 = \delta k_4 = 2\gamma_I(I_L + \theta I_R) \tag{39}$$

Equations 35 and 36 transform to [10]

$$\partial A_3/\partial z = -i\gamma_I D(I_L I_R)^{1/2}A_4^* \exp(i\kappa z) \tag{40}$$

$$\partial A_4/\partial z = -i\gamma_I D(I_L I_R)^{1/2}A_3^* \exp(i\kappa z) \tag{41}$$

with the propagation coefficient mismatch

$$\kappa = \Delta k - \delta k_L - \delta k_R + \delta k_3 + \delta k_4 = \begin{cases} \Delta k + \gamma_I(I_L + I_R) & \text{for } \omega_R \neq \omega_L \quad (42a) \\ \Delta k + 2\gamma_I I_L & \text{for } \omega_R = \omega_L \quad (42b) \end{cases}$$

The general solution of the equation system (40, 41) is

$$A_3(z) = [a_3 \exp(gz) + b_3 \exp(-gz)] \exp[i\kappa z/2] \tag{43}$$

$$A_4(z) = [a_4 \exp(gz) + b_4 \exp(-gz)] \exp[i\kappa z/2] \tag{44}$$

with

$$g = \left(\gamma_I^2 D^2 I_L I_R - \kappa^2/4\right)^{1/2} \tag{45}$$

where a_3, b_3, a_4, b_4 are parameters depending on the initial conditions and g is the parametric gain coefficient.

For stimulated four-photon mixing (start from noise, $I_3(0) = I_4(0) = I_N$) and para-

metric four-photon amplification ($I_3(0) \neq 0$, $I_4(0) = 0$) the light intensities at the fibre output are

$$I_3 = I_3(0)\left[\theta_3 + (\gamma_I^2 D^2 I_L I_R / g^2)\sinh^2(gl)\right] \tag{46}$$

$$I_4 = I_3(0)(\gamma_I^2 D^2 I_L I_R / g^2)\sinh^2(gl) \tag{47}$$

where $\theta_3 = 0$ in the case of stimulated four-photon mixing and $\theta_3 = 1$ in the case of parametric four-photon amplification. If g is imaginary, no parametric amplification occurs (no increase of signal at ω_3 and ω_4) but a transfer of signal from ω_3 to ω_4 is possible according to

$$I_4 = I_3(0)(\gamma_I^2 D^2 I_L I_R / |g^2|)\sin^2(|g|l) \tag{48}$$

for $I_3(0) \neq 0$.

In fibres, the wave vector mismatch Δk has contributions from the material dispersion, Δk_M, and from the waveguide dispersion Δk_W [4, 11], i.e.

$$\Delta k = \Delta k_M + \Delta k_W \tag{49}$$

For the interactions (I) $\omega_L + \omega_L \rightarrow \omega_3 + \omega_4$ and (II) $\omega_L + \omega_R \rightarrow \omega_3 + \omega_4$ the material wave vector mismatch is given by

$$\Delta k_M(\mathrm{I}) = (1/c_0)(n_3\omega_3 + n_4\omega_4 - 2n_L\omega_L) \tag{50a}$$

$$\Delta k_M(\mathrm{II}) = (1/c_0)(n_3\omega_3 + n_4\omega_4 - n_L\omega_L - n_R\omega_R) \tag{50b}$$

and the waveguide wave vector mismatch is [4, 11]

$$\Delta k_W(\mathrm{I}) = (1/c_0)\left[(n_{3,m3} - n_3)\omega_3 + (n_{4,m4} - n_4)\omega_4 - (n_{L,mL1} - n_L + n_{L,mL2} - n_L)\omega_L\right] \tag{51a}$$

$$\Delta k_W(\mathrm{II}) = (1/c_0)\left[(n_{3,m3} - n_3)\omega_3 + (n_{4,m4} - n_4)\omega_4 - (n_{L,mL} - n_L)\omega_L - (n_{R,mR} - n_R)\omega_R\right] \tag{51b}$$

where the $n_{i,mi}$ are the effective refractive indices of the fibre modes m_i at frequency ω_i [11, 21]. The n_i are the refractive indices of the core material (silica glass in our case).

The material wave vector mismatch $\Delta k_M(\mathrm{I})$ is shown by the dashed curve 1 in Fig. 11. It is $\Delta k_M(\mathrm{I}) \geq 0$ over the whole displayed wavelength region.

In polarization-preserving birefringent monomode fibres the refractive indices of the fundamental mode HE_{11} in the x-direction (n_x) and y-direction (n_y) are different, leading to a waveguide wave vector mismatch contribution δk_W depending on the polarizations of the modes at $\omega_3, \omega_4, \omega_L$, and ω_R. The interaction (I) $\omega_L + \omega_L \rightarrow \omega_3 + \omega_4$ may be phase-matched by this modal birefringence [4, 41, 48, 49]. In non-polarization-preserving monomode fibres either it is $n_x = n_y$ or the birefringence contributions average out over some distance, leading to $\delta k_W = 0$. In these monomode fibres it is $|\Delta k_W| \ll |\Delta k_M|$ so that $\Delta k \approx \Delta k_M$ and the propagation coefficient mismatch for the interaction (I) $\omega_L + \omega_L \rightarrow \omega_3 + \omega_4$ reduces to

$$\kappa(\mathrm{I}) = \Delta k_M(\mathrm{I}) + 2\gamma_I' I_L \tag{52}$$

The dashed curves in Fig. 11 show $\kappa(\mathrm{I})$ for some laser intensities. Insertion of Equation 52 into Equation 45 shows that the parametric gain coefficient g is always imaginary and therefore no stimulated four-photon mixing or parametric amplification occurs by

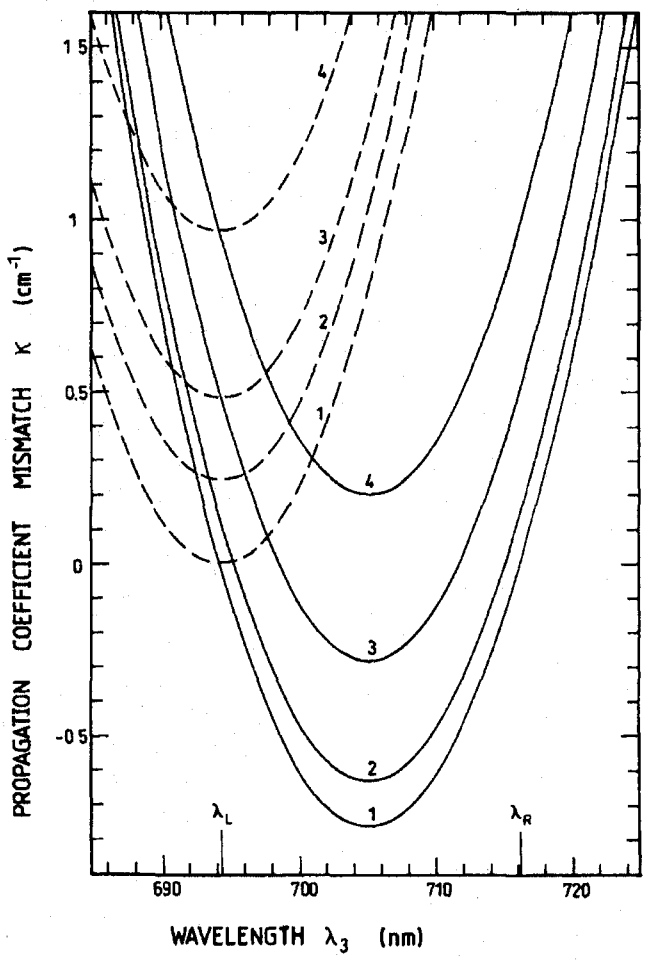

Figure 11 Wavelength dependence of the propagation coefficient mismatch κ (Equation 42). Dashed curves, type I interaction $\omega_L + \omega_L \rightarrow \omega_3 + \omega_4$. Solid curves, type II interaction $\omega_L + \omega_R \rightarrow \omega_3 + \omega_4$ ($\tilde{\nu}_R = \tilde{\nu}_L - 440\,\text{cm}^{-1}$). Δk_W is neglected, i.e. $\Delta k = \Delta k_M$. Situation of non-polarization-maintaining fibre is considered. (1) $I_L = 0$ giving $\kappa = \Delta k_M$ (2) $I_L = 5 \times 10^9\,\text{W cm}^{-2}$, (3) $I_L = 1 \times 10^{10}\,\text{W cm}^{-2}$, and (4) $I_L = 2 \times 10^{10}\,\text{W cm}^{-2}$.

the interaction $\omega_L + \omega_L \rightarrow \omega_3 + \omega_4$. This situation applies to the investigated fibres no. 1 (core diameter 4 μm) and no. 2a (core diameter 5 μm).

For low-order-mode fibres (fibre no. 3 with core diameter of 8 μm, and fibre no. 2b) various modes at ω_L, ω_3, and ω_4 may propagate and $\Delta k_W(\text{I})$ may become sufficiently negative to compensate $\Delta k_M(\text{I}) + 2\gamma_I' I_L$. Therefore $\kappa(\text{I}) = 0$ may be achieved at certain wavelengths and intensity values. The maximum value of the parametric gain coefficient g becomes (Equation 45)

$$g_{\max}(\text{I}) = \gamma_I I_L = g_P I_L \tag{53}$$

where $g_P = \gamma_I$ is the peak parametric gain factor. For non-polarization-maintaining fibres g_P has to be replaced by $g_P' = (5/6)g_P$ [38]. At phase-matched wavelengths the threshold intensity of efficient stimulated four-photon mixing is [4, 6]

$$I_{P,\text{th}} = 16/g_P L_P = 16/\gamma_I L_P \tag{54}$$

where $L_P = \min[L_w(\lambda_3), l]$ is the effective interaction length of stimulated four-photon

interaction. Since g_P is larger than g_R (see Table II) it is expected that under phase-matched conditions the stimulated parametric four-wave mixing starts before the stimulated Raman scattering. This behaviour was observed for the 8-μm core fibre (no. 3) and the 5-μm core fibre of 50 m length (no. 2b). The appearance of signal and idler components before the onset of stimulated Raman scattering is clearly seen in Fig. 3b.

In multimode fibres (nos 4 to 6) the effective refractive indices of the dominant low-order modes approach the core refractive indices [11, 21] and Δk_W becomes negligibly small. Phase-matched type I parametric amplification ($\omega_L + \omega_L \rightarrow \omega_3 + \omega_4$) is not expected and has not been observed experimentally.

The material wave vector mismatch $\Delta k_M(II)$ for the interaction $\omega_L + \omega_R \rightarrow \omega_3 + \omega_4$ ($\tilde{\nu}_R = \tilde{\nu}_L - \delta\tilde{\nu}_R, \delta\tilde{\nu}_R = 440\,\text{cm}^{-1}$) is shown by the solid curve 1 in Fig. 11. $\Delta k_M(II)$ is negative in the wavelength region between λ_L and λ_R. The other solid curves in Fig. 11 present the propagation coefficient mismatch $\kappa(II) = \Delta k_M + \gamma_I'(I_L + I_R)$ (Equation 42a) for some values of $I_L = I_R$. The waveguide wave vector mismatch Δk_W is neglected.

For the nondegenerate interaction $\omega_L + \omega_R \rightarrow \omega_3 + \omega_4$ (II) stimulated four-wave mixing and parametric amplification is possible (g real) in a certain (intensity-dependent) wavelength region. In Fig. 12 the parametric gain coefficient g is plotted versus wavelength for various laser intensities I_L and Raman intensity factors $\beta_R = I_R/I_L = 1$ (solid curves) and $\beta_R = 0.1$ (dashed curves). For sufficiently large I_L and β_R values the parametric gain region spans the full wavelength region between λ_L and λ_R and extends

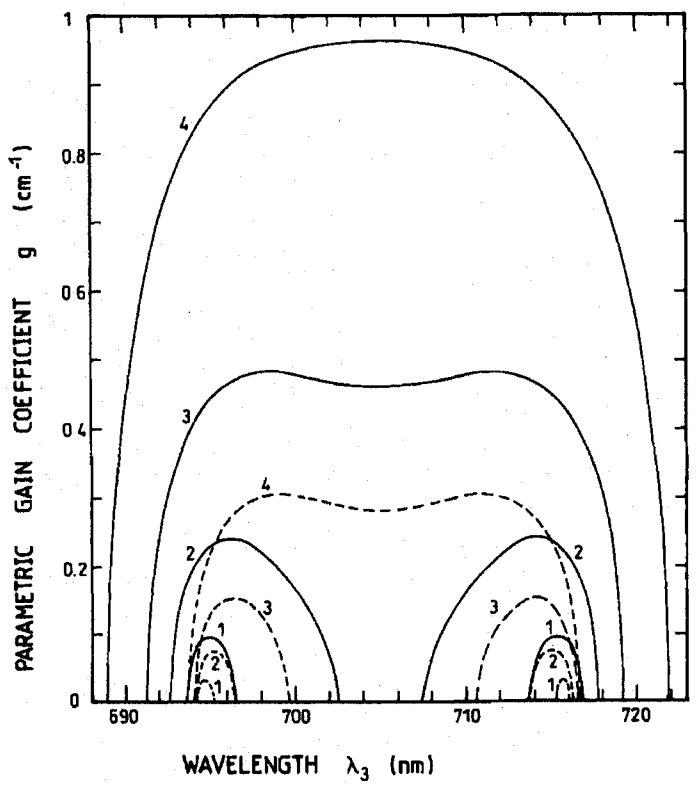

Figure 12 Parametric gain coefficient g (Equation 45) for type II interaction $\omega_L + \omega_R \rightarrow \omega_3 + \omega_4$ versus wavelength. Situation of non-polarization-maintaining fibre is considered. Solid curves, intensity ratio $\beta_R = I_R/I_L = 1$ Dashed curves, $\beta_R = 0.1$. (1) $I_L = I_{R,th,min} = 16/(g'_R L_{w,R}) = 2 \times 10^9\,\text{W cm}^{-2}$ (Equation 20), (2) $I_L = 5 \times 10^9\,\text{W cm}^{-2}$, (3) $I_L = 1 \times 10^{10}\,\text{W cm}^{-2}$, and (4) $I_L = 2 \times 10^{10}\,\text{W cm}^{-2}$.

slightly beyond λ_L and λ_R. At low intensities the parametric amplification is restricted to the Stokes vicinity of the laser wavelength and the anti-Stokes vicinity of the Raman wavelength. This location of the parametric signal is clearly seen in Fig. 4a (125-μm core fibre).

The maximum parametric amplification $G_{max} = g_{max} L_R$ may be estimated from Equation 45 by setting $\kappa = 0$ and $I_L = I_R = 16/g'_R L_R$, which gives $G_{max} = 32\gamma'_I/g'_R \approx 55$ (higher intensities or longer interaction lengths are not expected because of pump pulse depletion and light conversion to higher Stokes Raman components). The value of G_{max} shows that under favourable conditions efficient nondegenerate stimulated four-photon mixing may occur. Efficient parametric amplification of Raman light generated over a broad spectral region (spontaneous Raman spectrum is very broad [12]) may occur already before the onset of efficient stimulated four-photon mixing. Especially broad spectral distributions were obtained experimentally for the low-order-mode fibre no. 3 (core diameter 8 μm) where the processes of type I stimulated four-photon mixing [$\Delta k_W(\mathrm{I}) < 0$], stimulated Raman scattering, and type II parametric generation and amplification act simultaneously. When $I_{P,th} < I_{R,th}$ then Raman amplification of the parametric light in the Raman gain region may enhance the signal as is seen in Fig. 7c.

4.7. Self-focusing

In bulk media the self-focusing length of spatial Gaussian pulses due to the nonlinear refractive index is [50]

$$z_f = \frac{\omega_L r_{0L}^2}{c_0} \frac{1}{[(P_L/P_{cr}) - 1]^{1/2} + \theta_D} \tag{55}$$

where r_{0L} is the 1/e radius of the laser intensity (r_{0L} is approximately equal to the effective core radius a_{eff} [31]), θ_D is the divergence angle of the incident light, $P_L = \pi r_{0L}^2 I_{0L} = 2(\ln 2)^{1/2} W_L/(\pi^{1/2} \Delta t_L)$ is the laser power, and W_L is the laser energy. The critical power necessary for the occurrence of self-focusing is

$$P_{cr} = \pi \epsilon_0 c_0^3 / 2 n_2 \omega_L^2 \tag{56}$$

and the critical energy is

$$W_{cr} = \pi^{1/2} \Delta t_L P_{cr} / 2(\ln 2)^{1/2} \tag{57}$$

For $P_L < P_{cr}$ or $W_L < W_{cr}$ no whole beam self-focusing can occur. P_{cr} and W_{cr} are listed in Table II. W_{cr} is indicated in Fig. 8 by a dash-dotted line. W_{cr} is larger than the Raman threshold energy $W_{R,th}$ for the fibres nos 1 to 4 and it is larger than the surface damage threshold energy $W_{sur,d}$ of the fibres nos 1 to 3. For the fibres nos 4 and 5 surface damage occurred before the indication of any self-focusing. The spatial beam profile seems to approach a rectangular pulse shape before self-focusing occurs. In the 600-μm core fibre, self-focusing occurred for input pulse energies $W_i \gtrsim 800\,\mu$J, showing up in a damage of the fibre core a few centimetres inside the fibre entrance. A self-focusing length of $z_f = 4.3$ cm is calculated for $W_i = 800\,\mu$J. The self-focusing and accompanied bulk material damage limits the output pulse energy of the 600-μm fibre to $W_o \lesssim 400\,\mu$J.

5. Conclusions

The spectral broadening of picosecond pulses of a passively mode-locked ruby laser in optical fibres has been investigated. In a 50-m-long monomode fibre a spectral broadening from $\Delta\tilde{\nu}_L \approx 0.6\,\mathrm{cm}^{-1}$ to $\Delta\tilde{\nu}_L \approx 50\,\mathrm{cm}^{-1}$ has been achieved before the onset of stimulated Raman scattering. A temporal pulse compression down to 0.35 ps should be possible. In a 4-m-long fibre of 8-μm core diameter rather smooth spectra have been generated extending from 685 nm to 830 nm by employing self-phase modulation, parametric four-photon interaction, stimulated Raman scattering, and spectral filtering with a ruby rod. The output pulse energy of the spectrally broadened pulses was varied between $\sim 10\,\mu$J for monomode fibres and $\sim 200\,\mu$J for a multimode fibre of 600 μm core diameter. The experimental results are in good agreement with theoretical expectations.

The spectrally broadened pulses may be applied as probe pulses in time-resolved and wavelength-resolved pump and probe spectroscopic experiments exploring the spectral region around the pump laser frequency.

Acknowledgements

The authors thank the Deutsche Forschungsgemeinschaft for financial support.

References

1. C. H. BRITO CRUZ, J P GORDON, P. C. BECKER, R. L. FORK and C. V. SHANK, *IEEE J. Quantum Electron.* **QE-24** (1988) 261.
2. W. E. MOERNER, A. R. CHRAPLYVY and A. J. SIEVERS, *Phys. Rev.* **B29** (1984) 6694.
3. Y. R SHEN and G.-Z. YANG, *The Supercontinuum Laser Source*, edited by R. R. Alfano (Springer-Verlag, New York, 1989) p. 1.
4. G P AGRAWAL, *Nonlinear Fiber Optics* (Academic Press, Boston, 1989).
5. P. L. BALDECK, P. P. HO, and R. R. ALFANO, *The Supercontinuum Laser Source*, edited by R. R. Alfano (Springer-Verlag, New York, 1989) p. 117.
6. R. H. STOLEN, *Proc. IEEE* **68** (1980) 1232.
7. R. H. STOLEN and C LIN, *Phys. Rev.* **A17** (1978) 1448.
8. S. C. PINAULT and M. J. POTASEK, *J. Opt. Soc. Am.* **B2** (1983) 1318.
9. G. P. AGRAWAL, *Phys. Rev. Lett.* **59** (1987) 880.
10. R. H. STOLEN and J. E. BJORKHOLM, *IEEE J. Quantum Electron.* **QE-18** (1982) 1062.
11. R. H STOLEN, J. E. BJORKHOLM and A. ASHKIN, *Appl. Phys. Lett.* **24** (1974) 308.
12. R. H. STOLEN, *IEEE J. Quantum Electron.* **QE-11** (1975) 100.
13. P. L. BALDECK and R. R. ALFANO, *J. Lightwave Technol.* **LT-5** (1987) 1712.
14. K. WASHIO, K. INOUE and S. KISHIDA, *Electron. Lett.* **16** (1980) 658.
15. P L. BALDECK, P P HO and R. R. ALFANO, *Rev. Phys. Appl.* **22** (1987) 1677.
16. A. M. JOHNSON and W. M. SIMPSON, *J. Opt. Soc. Am.* **B2** (1985) 619.
17. T. DAMM, M KASCHKE, F. NOACK and B. WILHELMI, *Opt. Lett.* **10** (1985) 176.
18. Q. Z WANG, D. LI, L. YANG, P. P. HO and R R. ALFANO, *Opt. Lett.* **14** (1989) 578.
19. A. M. JOHNSON and C V. SHANK, *The Supercontinuum Laser Source*, edited by R. R. Alfano (Springer-Verlag, New York, 1989) p. 399.
20. W RUDOLPH and B WILHELMI, *Light Pulse Compression* (Harwood Academic Publishers, Chur, 1989).
21. D. GLOGE, *Appl. Opt.* **10** (1971) 2252.
22. J. R. THOMPSON and R. ROY, *Phys. Rev.* **A43** (1991) 4987.
23. Y. CHEN, *J. Opt. Soc. Am.* **B7** (1990) 43.
24. D. B KECK, *Fundamentals of Optical Fiber Communications*, 2nd edn, edited by M. K. Barnoski (Academic Press, New York, 1981) p. 1.
25. A. J. GLASS and A. H. GUENTHER, *Appl. Opt.* **18** (1978) 2112.
26. W. KOECHNER, *Solid-State Laser Engineering*, 2nd edn (Springer-Verlag, Berlin, 1988) p. 540.
27. M J. SOILEAU, *Photonics Spectra* **21/11** (1987) 109.

28. I. N. SISAKYAN and A B. SHVARTSBURG, *Sov. J. Quantum Electron.* **14** (1984) 1146.
29. D COTTER, *Opt. Quantum Electron.* **19** (1987) 1.
30. C YEH, *Handbook of Fiber Optics. Theory and Applications* (Academic Press, San Diego, 1990).
31. D MARCUSE, *J. Opt. Soc. Am.* **68** (1978) 103.
32. I. H. MALITSON, *J. Opt. Soc. Am.* **55** (1965) 1205.
33. E. M DIANOV, L M IVANOV, P V. MAMYSHEV and A. M. PROKHOROV, *IEEE J. Quantum Electron.* **25** (1989) 828.
34. J. P. HERITAGE, A. M. WEINER, R. J. HAWKINS and O. E. MARTINEZ, *Opt. Commun.* **67** (1988) 367.
35. W. J. TOMLINSON, R. H. STOLEN and A. M. JOHNSON, *Opt. Lett.* **10** (1985) 457.
36. A. PENZKOFER and W. LEUPACHER, *Opt. Quantum Electron.* **20** (1988) 369.
37. P N. BUTCHER and D. COTTER, *The Elements of Nonlinear Optics* (Cambridge University Press, Cambridge, 1991).
38. R. H. STOLEN, *Optical Fiber Telecommunications*, edited by S. E. Miller and A. G. Chynoweth (Academic Press, New York, 1975) ch. 5, p. 125.
39. B. MEIER, P WEIDNER and A. PENZKOFER, *Appl. Phys.* **B51** (1990) 404.
40. R. R ALFANO and S. L. SHAPIRO, *Phys. Rev. Lett.* **24** (1970) 584.
41. R. H. STOLEN, M A. BOSCH and C. LIN, *Opt. Lett.* **6** (1981) 213.
42. C. LIN and M. A. BÖSCH, *Appl. Phys. Lett.* **38** (1981) 479.
43. K. WASHIO, K. INOUE and T. TANIGAWA, *Electron. Lett.* **16** (1980) 331.
44. A. PENZKOFER, A. LAUBEREAU and W. KAISER, *Phys. Rev. Lett.* **31** (1973) 863.
45. A. PENZKOFER and W KAISER, *Opt. Quantum Electron.* **9** (1977) 315.
46. A. LAUBEREAU, *Ultrashort Laser Pulses and Applications*, edited by W. Kaiser, Topics in Appl. Phys. Vol. 60 (Springer-Verlag, Berlin, 1988) p. 35.
47. I. BAR-JOSEPH, A. A. FRIESEM, R. G. WAARTS and H H YAFFE, *Opt. Lett.* **11** (1986) 534.
48. R. K. JAIN and K. STENERSEN, *Appl. Phys.* **B35** (1984) 49.
49. K. STENERSEN and R K. JAIN, *Opt. Commun.* **51** (1984) 121.
50. P. W MILONNI and J. H. EBERLY, *Lasers* (Wiley, New York, 1988) p. 709.
51. P. L. BALDECK, F. RACCAH and R. R. ALFANO, *Opt. Lett.* **12** (1987) 588.